Springer

Acta Mechanica Sinica

CrossMark click for updates

• RESEARCH PAPER •

Acta Mech. Sin., Vol. 41, 424434 (2025)
https://doi.org/10.1007/s10409-024-24434-x

A modified random sequential absorption algorithm for generating RVE of discontinuous curved fiber reinforced composites

Wujie Chen[1], Kunkun Fu[1,2*], and Yan Li[1,2*]

[1] *School of Aerospace Engineering and Applied Mechanics, Tongji University, Shanghai 200092, China;*
[2] *Shanghai Institute of Aircraft Mechanics and Control, Shanghai 200092, China*

Received August 28, 2024; accepted September 18, 2024; published online December 26, 2024

The present study proposes a modified random sequential absorption (RSA) algorithm to generate a representative volume element (RVE) model for predicting the elastic properties of discontinuous curved fiber reinforced composites (DCFRCs) with varying fiber waviness functions and orientations. A small-move method was proposed to modify the traditional RSA algorithm. In comparison with the original RSA algorithm, the generation efficiency of the proposed modified RSA algorithm increased by over 40%, and the achievable maximum fiber volume fraction could reach up to 15% with a fiber aspect ratio of 15. The generated RVE model was utilized in conducting finite element analysis to investigate the effect of fiber waviness and wavy functions on the elastic properties of DCFRCs. Finally, a modified rule-of-mixture was proposed to predict the elastic properties of DCFRCs with various fiber orientations. The results indicated that the elastic properties predicted by the modified rule-of-mixture were in good agreement with those obtained from the RVE model, thereby demonstrating its effectiveness.

Discontinuous curved fiber reinforced composites (DCFRCs), Representative volume element (RVE), Modified RSA algorithm, Modified rule-of-mixture, Elastic properties, Fiber waviness

Citation: W. Chen, K. Fu, and Y. Li, A modified random sequential absorption algorithm for generating RVE of discontinuous curved fiber reinforced composites, Acta Mech. Sin. 41, 424434 (2025), https://doi.org/10.1007/s10409-024-24434-x

1. Introduction

Discontinuous fiber reinforced polymer composites have been increasingly utilized in a variety of applications, including transportation [1], medical equipment [2], military [3], and sports equipment [4] due to their exceptional processability, low density, and excellent mechanical properties. In order to effectively design a composite structure, it is crucial to establish an accurate and efficient numerical model for predicting their mechanical properties.

The mechanical properties of a composite are significantly influenced by the mechanical properties of its reinforced fibers and matrices, as well as their microstructures. Various microstructural parameters have been identified as having significant effects on the elastic modulus of composites, including the fiber length-diameter ratio [5,6], the fiber orientation [7], and the fiber volume fraction [5,6]. It is worthwhile noting that the waviness of the fibers is a significant microstructural parameter, particularly noticeable with a large fiber length-to-diameter ratio. Figure 1(a) shows a microstructural image of a long fiber reinforced thermoplastic composite, where a considerable number of fibers exhibit prominent waviness. Another typical example can be observed in carbon nanotube (CNT) reinforced composites shown in Fig. 1(b), where the wavy nature of the carbon nanotube is clearly evident. The curved fibers may have a substantial impact on the mechanical properties of the composites.

To date, several analytical methods have been proposed to determine the mechanical properties of discontinuous curved fiber reinforced composites (DCFRCs). Bapanapalli and Nguyen [10] utilized the Eshelby-Mori-Tanaka model to calculate the stiffness matrix of a unit cell of composite

*Corresponding authors. E-mail address: 1984fukunkun@tongji.edu.cn (Kunkun Fu); liyan@tongji.edu.cn (Yan Li)
Executive Editor: Zhong Zhang

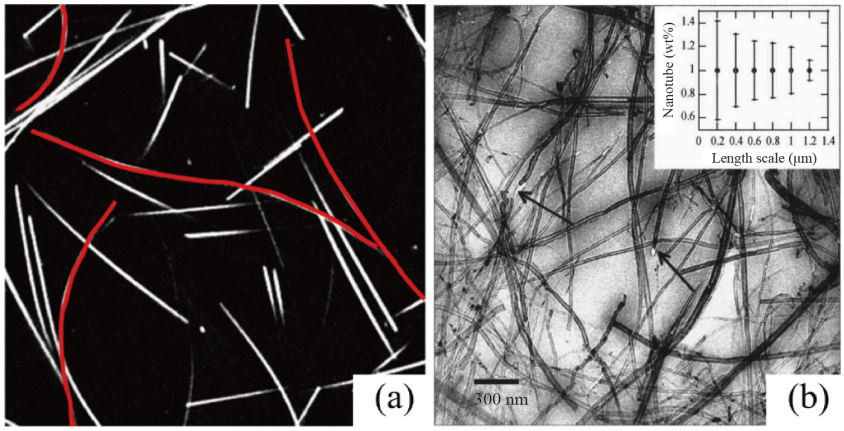

Figure 1 Microstructure. (a) Long fiber reinforced composite [8]; (b) CNT reinforced composite [9].

containing a curved fiber bundle with a half-sine wavy type. The effect of fiber waviness on the elastic modulus of the composites was accordingly examined. Tsai et al. [11] also developed an analytical method based on the Eshelby model. The influence of fiber waviness and distribution on the elastic properties of composites with three typical fiber orientation distributions including unidirectional, planar random (2D-random) and three-dimensional random (3D-random) distributions. Oller et al. [12] proposed a theoretical homogenized constitutive formulation to predict the elastic modulus of a composite with a half-sinusoidal wavy fiber. They discovered that the waviness of the fiber has a significant effect on the elastic properties of the composite. The aforementioned analytical methods only include a single type of fiber waviness when predicting the elastic modulus of DCFRCs, although the actual distribution and orientation of fibers are complex depended on manufacturing process.

The representative volume element (RVE) method has the capability to incorporate more complex fiber shapes and distributions within composites. The process of generating a typical RVE for DCFRCs can be mainly categorized into two methods. The first method assumes that the fiber waviness is distributed randomly. A common algorithm used for this purpose is the random-walk method, which can create an RVE with a high fiber volume fraction. In this method, the fiber is represented as chains of balls and the fiber waviness is assumed to be irregular and controlled by the random walk of these balls. For instance, Altendorf and Jeulin [13] utilized the random-walk method to generate an RVE with curved fibers. Originally they did not take into account fiber overlap and then employed a force-based method to separate the overlapped fibers. Herasati and Zhang [14] proposed a modified random-walk method to create an RVE of wavy CNTs by representing each wavy CNT as a series of 3D small straight segments. They established an RVE with a CNT volume fraction of 0.5% in order to investigate the impact of wavy CNTs on the elastic properties in CNT composites. Kumar et al. [15] proposed a modified random-walk algorithm capable of generating an RVE with straight, slightly wavy, and fully wavy shaped fibers. The maximum achieved fiber volume fraction of composites with aligned fibers using their method was 45.6% for fibers with a radius of 5 μm and an aspect ratio of 10. For a 3D uniform-random orientation state, they achieved the maximum fiber volume fraction of 41.8% for fibers with a radius of 3.6 μm and a length of 100 μm. Another RVE algorithm is the sequential addition and migration (SAM) algorithm [16]. This algorithm establishes an RVE with curved fibers by discretizing the curved fibers into multiple straight segments, with the fiber waviness controlled by the angle between the adjacent fiber segments. This approach could result in a fiber volume fraction of more than 10% and a maximum fiber aspect ratio of 240. In order to investigate the impact of fiber waviness on the mechanical properties of composites, it is essential to establish an RVE with a specific type of fiber waviness. However, controlling the fiber waviness precisely may be challenging for random-walk or SAM algorithms. Therefore, it may be necessary to develop an alternative method that assumes the fiber waviness follows a mathematical function.

Most of the researches have been focused on the development of RVEs with fibers exhibiting sinusoidal or cosinoidal waviness. For instance, Velmurugan et al. [17] employed an RVE to investigate the influence of fiber waviness on the stiffness of composites containing curved fibers. The fibers were assumed to possess a sinusoidal wavy pattern, and only a unidirectional fiber state was taken into consideration.

Zhang et al. [18] developed a novel RVE builder combined with rigid body dynamics simulation to construct 3D RVEs with random/aligned wavy CNTs at three different volume fractions, i.e., 1.5%, 3.0%, and 4.5%. In this study, the fibers were assumed to be full-sinusoidal wavy type. Their results also indicated that this method has the ability to generate an RVE with a fiber volume content of 10% for a

3D-random orientation state with a fiber aspect ratio of 30. Furthermore, Abdin et al. [19] proposed a method for generating RVEs of curved short fiber reinforced composites, which describes fiber waviness using a mathematical function. This method is capable of generating RVEs with various complex types of fiber waviness. However, their study only achieved a fiber volume fraction of 0.05% in the generated RVE, which is significantly lower compared to industrial composites. Therefore, it is essential to develop a new algorithm for generating RVEs of DCFRCs that can achieve relatively high fiber volume fractions while maintaining specific wavy types and orientation states as required in industrial applications.

The RVE model is widely acknowledged for its exceptional accuracy in predicting the elastic modulus of composites. However, the calculation process can be extensive and the modeling is complex, making it unsuitable for large-scale engineering calculations. In contrast, the rule of mixture (ROM) can be utilized to predict the elastic properties of composites, typically demonstrating a relatively high level of computational efficiency. Typical ROM includes Cox model [20], Halpin-Tsai model [21] and Chamis model [22]. The Cox model offers the compute method for longitudinal modulus of unidirectional straight discontinuous fiber reinforced composites as

$$\begin{cases} E_{\mathrm{L}}^{\mathrm{straight}} = \eta_{\mathrm{L}} E_{\mathrm{f}} V_{\mathrm{f}} + E_{\mathrm{m}}(1 - V_{\mathrm{f}}), \\ \eta_{\mathrm{L}} = 1 - \dfrac{\tanh\left(\dfrac{\beta L}{2}\right)}{\dfrac{\beta L}{2}}, \end{cases} \tag{1}$$

where

$$\beta = \left[\frac{2G_{\mathrm{m}}}{E_{\mathrm{f}} r_0^2 \ln(r_1/r_0)}\right]^{\frac{1}{2}}, \tag{2}$$

where $E_{\mathrm{L}}^{\mathrm{straight}}$ is the longitudinal modulus of straight discontinuous fiber composites. η_{L} is the fiber length efficiency factor. E_{f} and E_{m} are the elastic modulus of fiber and matrix. V_{f} is the fiber content fraction. L denotes the fiber length. G_{m} is the shear modulus of resin. r_0 is the fiber radius. r_1 is a parameter which is related to the fiber alignment and fiber content.

Halpin-Tsai model gives the prediction formulas of the longitudinal and transverse modulus of unidirectional straight discontinuous fiber reinforced composites as

$$\begin{cases} E_{\mathrm{L}}^{\mathrm{straight}} = \dfrac{1 + \dfrac{L}{r_0}\eta_{\mathrm{L}} V_{\mathrm{f}}}{1 - \eta_{\mathrm{L}} V_{\mathrm{f}}} E_{\mathrm{m}}, \\ E_{\mathrm{T}}^{\mathrm{straight}} = \dfrac{1 + 2\eta_{\mathrm{T}} V_{\mathrm{f}}}{1 - \eta_{\mathrm{T}} V_{\mathrm{f}}} E_{\mathrm{m}}, \end{cases} \tag{3}$$

where

$$\eta_{\mathrm{L}} = \frac{E_{\mathrm{f}}/E_{\mathrm{m}} - 1}{E_{\mathrm{f}}/E_{\mathrm{m}} + L/r_0}, \ \eta_{\mathrm{T}} = \frac{E_{\mathrm{f}}/E_{\mathrm{m}} - 1}{E_{\mathrm{f}}/E_{\mathrm{m}} + 2}. \tag{4}$$

For 2D-random and 3D-random distributions, there are empirical formulas for calculating the elastic modulus of straight discontinuous fiber reinforced composites as [23,24]

$$\begin{cases} E_{\mathrm{c}}^{\mathrm{straight}} = \dfrac{3}{8} E_{\mathrm{L}}^{\mathrm{straight}} + \dfrac{5}{8} E_{\mathrm{T}}^{\mathrm{straight}}, & \text{2D-random}, \\ E_{\mathrm{c}}^{\mathrm{straight}} = \dfrac{1}{5} E_{\mathrm{L}}^{\mathrm{straight}} + \dfrac{4}{5} E_{\mathrm{T}}^{\mathrm{straight}}, & \text{3D-random}, \end{cases} \tag{5}$$

where $E_{\mathrm{L}}^{\mathrm{straight}}$ and $E_{\mathrm{T}}^{\mathrm{straight}}$ denote the longitudinal and transverse modulus for unidirectional straight discontinuous fiber composites with the same fiber diameter, aspect ratio and fiber content, respectively.

Up to now, the majority of existing ROM methods have been proposed for predicting the elastic properties of straight fiber reinforced composites. Limited ROMs have been proposed to predict the elastic modulus of DCFRCs.

In this study, we present a modified random sequential absorption (RSA) algorithm for generating the RVE of DCFRCs. We propose a small-move method to enhance the algorithm's generation efficiency, enabling it to generate RVEs with a fiber volume fraction of up to 15% and a fiber aspect ratio of up to 15. Spline curves based on mathematical formulations are utilized to describe the shape of fibers, ensuring both fiber continuity and easy control of fiber waviness. Furthermore, we investigate the influence of fiber waviness and wavy functions on composite properties. Finally, we propose a ROM specifically tailored for DCFRCs and conduct comparisons with RVE results to demonstrate the effectiveness of the ROM.

2. Descriptions of RVE algorithm

2.1 Modeling of curved fiber

A global coordinate system for a typical curved fiber in a three-dimensional space is illustrated in Fig. 2. The curved fiber is mathematically represented by a half-sine function as

$$y = A\sin\left(\frac{\pi}{L}x\right), \tag{6}$$

where A is the wavy amplitude. L is the wavelength, which means the end-to-end distance of a fiber. x represents the

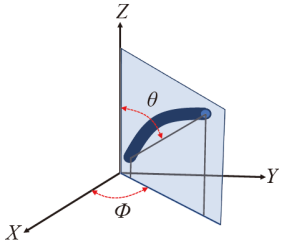

Figure 2 Modeling of curved fiber.

distance along the fiber direction, θ and Φ are the Euler angles of fiber.

The waviness of the curved fiber is controlled by its central axis, which is accurately represented using a spline curve to ensure fiber continuity. The orientation distribution of the fibers is described utilizing the second-order fiber-orientation tensor

$$A_{\text{ori}} = \text{diag}(a_1, a_2, a_3), \tag{7}$$

where $a_1 + a_2 + a_3 = 1$.

First, in order to describe the fiber waviness, a local coordinate system is established with the origin located at the starting point of a fiber, and the X-axis defined by the line connecting its start and end points, as depicted in Fig. 3, The fiber waviness is exclusively considered within the XOY plane of the local coordinate system. The specified drawing-points along the central axis are then utilized for sweeping to obtain the geometry of the curved fiber.

The curved line connecting the start point and end point is then divided into N equal parts, and the X-coordinates of drawing-points in local coordinate system are determined as specified

$$x_i = \frac{i \cdot L}{N},\ (i = 0, \ldots, N). \tag{8}$$

Thus, the local coordinates of each drawing-point can be obtained as

$$\left[X_i^{\text{local}}\right]_{\text{drawing-point}} = \left[\frac{i \cdot L}{N}, f\left(\frac{i \cdot L}{N}\right)\right]^{\text{T}},\ (i = 0, \ldots, N), \tag{9}$$

where $f(x)$ represents the mathematical function which describes the fiber waviness.

The X-axis and Y-axis of the local coordinate system are set as the same axes of the global coordinate system. Then, the global coordinates of each drawing-point can be obtained as

$$\begin{aligned}\left[X_i^{\text{global}}\right]_{\text{drawing-point}} &= \left[x_i, f(x_i), 0\right]^{\text{T}} \\ &= \left[\frac{i \cdot L}{N}, f\left(\frac{i \cdot L}{N}\right), 0\right]^{\text{T}},\ (i = 0, \ldots, N).\end{aligned} \tag{10}$$

The initial global coordinates of each control point are then calculated by rotating the drawing-points 90° clockwise around the Y-axis using the Eq. (11). In this scenario, both of the Euler angles of fiber (θ and Φ) are equal to zero and the starting point of the fiber is located at the origin. Subsequently, the global coordinates of control points at each fiber are obtained through coordinate transformation with varying θ and Φ

$$\begin{aligned}X_i^{\text{initial}} &= \begin{bmatrix} 0 & 0 & -1 \\ 0 & 1 & 0 \\ 1 & 0 & 0 \end{bmatrix} \left[X_i^{\text{global}}\right]_{\text{drawing-point}} \\ &= \left[0, f\left(\frac{i \cdot L}{N}\right), \frac{i \cdot L}{N}\right]^{\text{T}},\ (i = 0, \ldots, N).\end{aligned} \tag{11}$$

This method ensures the continuity of fibers throughout the entire axis and directly controls the waviness of the fibers using a mathematical function $y = f(x)$. All fibers are confined within the RVE in order to maintain the geometric periodicity of the RVE.

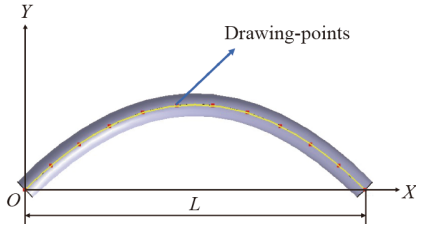

Figure 3 Local coordinate system for curved fiber.

2.2 Detection of fiber overlap

The detection of overlap is a crucial step in the RSA algorithm. By establishing control points along the fiber axis, not only can direct control over fiber waviness be achieved, but also a convenient numerical solution for detecting fiber overlap can be obtained. The main procedure is listed as:

i) The final coordinates of each control point in the global coordinate system can be obtained by performing a coordinate transformation using spatial position information;

$$\begin{cases} X_i^{\text{final}} = TX_i^{\text{initial}} + (x', y', z')^{\text{T}}, \\ X_i^{\text{final}} = (x, y, z)^{\text{T}}, \\ X_i^{\text{initial}} = \left[0, f\left(\frac{i \cdot L}{N}\right), \frac{i \cdot L}{N}\right]^{\text{T}}, \end{cases} (i = 0, 1, 2, 3, \ldots, N), \tag{12}$$

where X_i^{final} is the final global coordinates of i-th control point after coordinate transformation. X_i^{initial} is the initial global coordinates of i-th control point. $(x', y', z')^{\text{T}}$ represents the location coordinates in global coordinate system of the fiber. The coordinate transformation matrix T can be obtained from the orientation angles (Φ, θ) of the fiber by

$$T = \begin{bmatrix} \cos\Phi & -\sin\Phi & 0 \\ \sin\Phi & \cos\Phi & 0 \\ 0 & 0 & 1 \end{bmatrix} \times \begin{bmatrix} \cos\theta & 0 & \sin\theta \\ 0 & 1 & 0 \\ -\sin\theta & 0 & \cos\theta \end{bmatrix}. \tag{13}$$

ii) Computing the minimum distance between control points of the m-th fiber and control points of the k-th fiber;

$$\min\left|X_i^m, X_j^k\right|, (i, j = 0, 1, 2, 3, \ldots, N,\ m \in N^+,\ k \in N^+), \tag{14}$$

where X_i^m is the global coordinates of i-th control point of m-th fiber. X_j^k is the global coordinates of j-th control point of k-th fiber. $\left|X_i^m, X_j^k\right|$ is the distance between these two points (Fig. 4).

Obviously, the use of more control points leads to a more

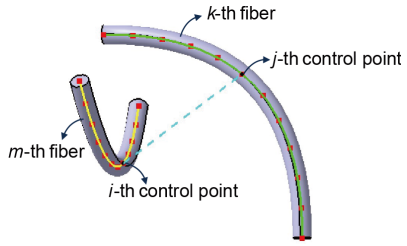

Figure 4 Overlap detection.

precise calculation of the minimum distance. For this study, the number of control points is set as 50.

iii) Determining the occurrence of overlap by comparing the minimum distance with the fiber diameter.

$$\begin{cases} \min\left|X_i^m, X_j^k\right| > \dfrac{d_i+d_j}{2}: \text{No overlap}, \\ \min\left|X_i^m, X_j^k\right| \leqslant \dfrac{d_i+d_j}{2}: \text{Overlapped}, \end{cases}$$
$$(i,j = 0,1,2,3,...,N, m \in N^+, k \in N^+), \tag{15}$$

where d represents the diameter of the fiber. A minimum distance of 5% of the fiber diameter is utilized to prevent fiber overlap resulting from numerical calculation errors and to avoid distortion of the meshed elements.

2.3 Modeling algorithm

The algorithm proposed in Fig. 5(a) utilizes the modeling and overlap detection method mentioned earlier to generate RVEs of DCFRCs. It is widely recognized that the RSA algorithm encounters challenges in generating RVE with high fiber volume content. Especially as the number of fibers increases, finding the next suitable fiber becomes challenging. Once fiber overlap is detected, it necessitates re-searching for the appropriate fiber in the entire RVE region, resulting in low generation efficiency. Therefore, we propose a small-move method to optimize the original algorithm. As illustrated in Fig. 5(b), once the overlap of fibers is detected, instead of discarding the generated fiber and searching for a new one, a small move of (Δx, Δy) is applied to the local coordinates of drawing-points of the overlapped fiber until the overlapping is resolved or the maximum number of moves (N_max) is reached. The optimization parameters (Δx, Δy and N_max) were set as

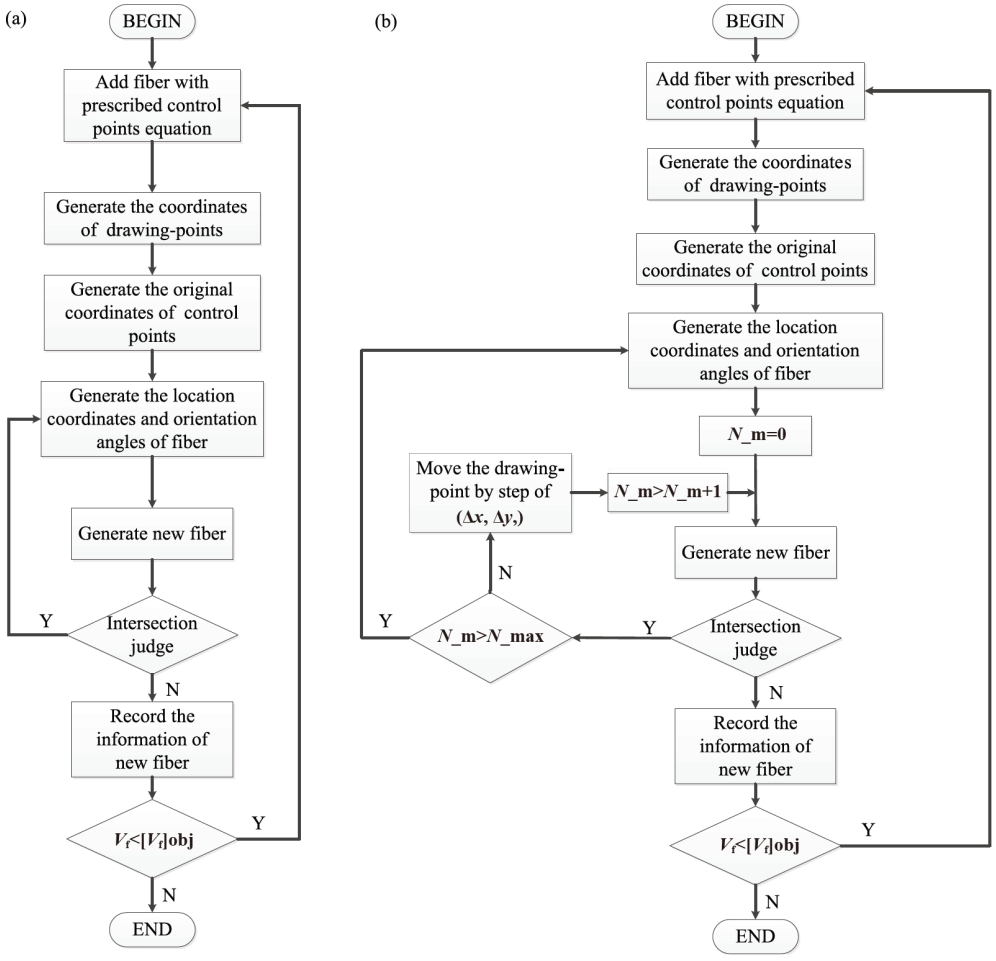

Figure 5 Modeling algorithm for CDFRCs. (a) Original algorithm; (b) modified algorithm.

$$\begin{cases} \Delta x = \Delta y = d_{\mathrm{f}} / 5, \\ N\_\max = 10, \end{cases} \tag{16}$$

where d_{f} represents the fiber diameter.

By conducting an RVE analysis of the same DCFRCs, the completion times of these two algorithms were compared using the same computer. Equation (6) was utilized to describe the fiber control points, with A set at 5 and L set at 105. The fiber diameter was specified as 7, and a 3D-random orientation distribution with a fiber volume fraction of 10% was taken into consideration. For each algorithm, the generation process was repeated three times, and the completion times were recorded. As shown in Table 1, the modified algorithm exhibits higher generation efficiency when producing RVEs with a relatively higher volume content (10%) compared to the original algorithm. The average generation time is reduced by over 40%.

Compared to the original algorithm, the modified algorithm is capable of generating RVEs with higher fiber volume content. For instance, Fig. 6 illustrates the generated RVEs of DCFRCs with a volume fraction of 15% in various orientation states and wavy types. In Fig. 6(a), the depicted RVE represents the composite with a half-sine wavy type in a unidirectional orientation state, characterized by an orientation tensor of diag (1, 0, 0). In Fig. 6(b), the RVE represents a composite with 3/4-sine wavy type in a 2D-random orientation state where the orientation tensor is diag (1/2, 1/2, 0). Figure 6(c) illustrates the RVE with a full-sine wavy type in a 3D-random orientation state denoted by an orientation tensor of diag (1/3, 1/3, 1/3). Figure 6(d) shows a random-oriented RVE containing a mixture of full-sine and half-sine wavy fibers as represented by an orientation tensor of diag (0.7, 0.22, 0.08).

2.4 Finite Element (FE) analysis

A commercial FE software ABAQUS was utilized to perform the FE analysis of RVEs. Previous studies [25-27] had demonstrated that using an RVE length equal to twice the fiber length is appropriate for determining the elastic properties of composites, which was also applied in this study. Periodic boundary conditions (PBCs) were employed in the RVE model to evaluate the elastic properties of the composites.

The geometry meshing utilized tetrahedral elements, resulting in the creation of a free-type mesh as shown in Fig. 7. To ensure convergence, a mesh convergence study was conducted by dividing the fiber circumference into 2 to 10 segments while employing 21 segments for the matrix edges. An RVE with curved fibers comprising approximately 2% volume fraction under a half-sine wavy pattern was utilized. The corresponding FE models consisted of element numbers ranging from 76,541 to 913,692. As shown in Fig. 8, the results of the mesh convergence study indicated that achieving at least four segments for dividing the fiber circumference led to converging values for elastic modulus. Consequently, further FE simulations were performed by subdividing the fiber circumference into more than four segments.

The study investigated the impact of fiber waviness and wavy functions on the mechanical properties of curved fiber reinforced composites. According to the studies of Chanda et al. [26], sinusoidal functions are a common characteristic of fiber waviness in DCFRCs. Therefore, this study considered three types of fiber waviness: half-sine, 3/4-sine, or full-sine. As shown in Fig. 9, three waviness functions are included: half-sine, 3/4-sine, and full-sine types.

The composite utilized in this study was a carbon fiber reinforced epoxy composite. The diameter of the carbon fibers was set at 7 μm, while their length ranged from 105 μm. The elastic properties of these two constituent materials are presented in Table 2.

3. Results and analysis

3.1 Model validation

To validate the accuracy of the FE results, existing experimental results of CNTs reinforced composites were compared with the FE predictions of the established RVE. The

Table 1 Comparison of generation time of two algorithms

No.	Original algorithm	Modified algorithm
1	109 (min)	61 (min)
2	112 (min)	59 (min)
3	102 (min)	50 (min)

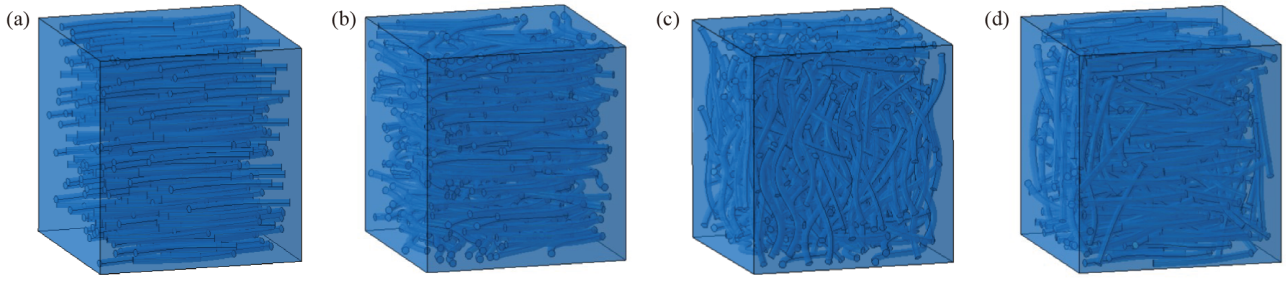

Figure 6 RVEs of CDFRCs with an orientation tensors. (a) Diag (1, 0, 0); (b) diag (1/2, 1/2, 0); (c) diag (1/3, 1/3, 1/3); (d) diag (0.7, 0.22, 0.08).

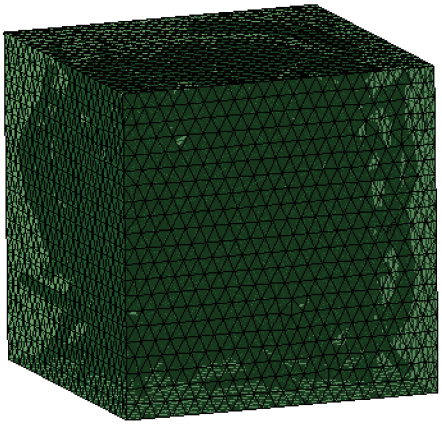

Figure 7 FE model of RVE.

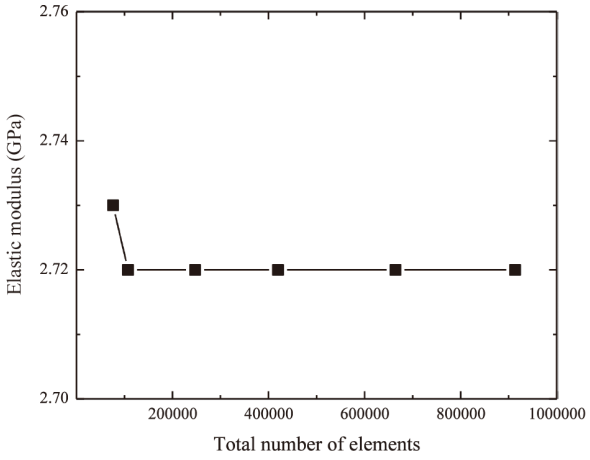

Figure 8 Mesh convergence study.

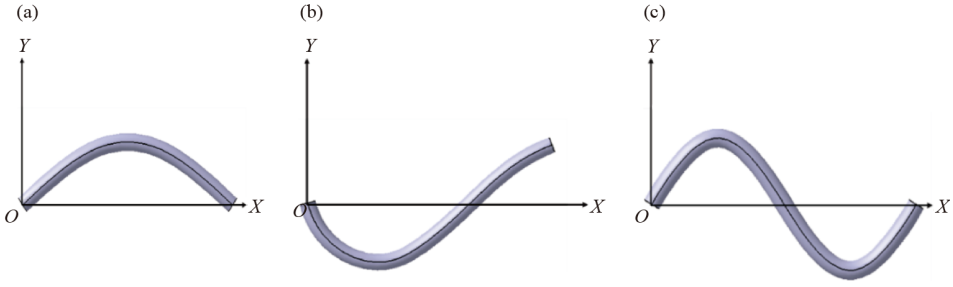

Figure 9 Fiber wavy types. (a) Half-sine; (b) 3/4-sine; (c) full-sine.

material is a low density polyethylene (LDPE) resin-based composite reinforced by multi-walled carbon nanotubes (MWCNTs), the material properties of CNTs reinforced composites for the validation study are listed as Table 3.

The raw granules of LDPE and MWCNTs were mixed at 140 °C for 20 min utilizing a mixer at the speed of 120 r min^{-1}, the molding pressure is 8 MPa and the molding was repeated 10 times to ensure that the nanotubes were evenly dispersed in the matrix [29]. The tensile properties of the molded dog bone specimens were tested at a crosshead rate of 100 mm min^{-1} using an Instron machine according to D638 standard [29].

According to the manufacturing process of the CNT reinforced composite sample, an orientation tensor of diag (1/3, 1/3, 1/3) is selected, representing a 3D-random orientation state. And the mathematical function of CNTs is simplified as a half-sine equation as [28]

$$y = 23.48\sin\left(\frac{\pi}{125.76}x\right). \tag{17}$$

RVEs with CNTs weight content of 1% and 3% were established, as illustrated in Fig. 10.

The error percentage between the RVE results and the experimental results is listed in Table 4. It is evident that there is a good agreement between the RVE results and the experimental ones with an error less than 7%, thereby validating the accuracy of the proposed RVE method.

Table 2 Elastic properties of constituent materials

Material	E (GPa)	v
Carbon fiber	230	0.25
Epoxy	2.48	0.3

Table 3 Material properties of CNTs composite used for validation study [28]

Parameter	Value
E_f (GPa)	1260
v_f	0.27
E_m (GPa)	0.235
v_m	0.46

3.2 Effect of fiber waviness

In this section, the influence of fiber waviness on the elastic properties of composites is analyzed under different orientation states. Three commonly adopted orientation states [14,29] are considered: (1) unidirectional, (2) 2D-random distribution state, and (3) 3D-random distribution state. The fiber content is maintained at a constant level of 10%, and the wavy functions for each type of waviness are listed as

(1) Half-sine: $y = A\sin\left(\frac{\pi}{L}x\right)$,

(2) 3/4-sine: $y = -A\sin\left(\frac{3\pi}{2L}x\right)$,

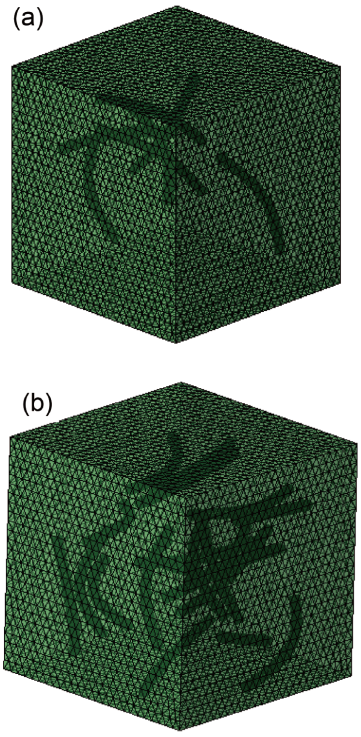

Figure 10 RVEs with different CNTs weight content. (a) 1%; (b) 3%.

Table 4 Percentage difference between RVE results and the experiment results

Fiber content (wt %)	Experiment results [29] (MPa)	RVE results (MPa)	Error percentage (%)
1	261	245	6
3	284	271	5

(3) Full-sine: $y = A\sin\left(\frac{2\pi}{L}x\right)$.

The elastic properties of the composites are determined as a function of fiber waviness in different orientation states, as illustrated in Figs. 11-13. Our findings demonstrated a significant influence of fiber waviness on the elastic properties of aligned fiber composites. An increase in fiber waviness leads to a decrease in E_{11} while causing an increase in G_{12} and E_{22}. E_{11} is most sensitive to the fiber waviness for aligned fiber composites. Particularly, E_{22} is significantly affected by large fiber waviness. However, v_{12} initially increases and then decreases with increasing the fiber waviness. Therefore, when the fibers have an aligned distribution, the prediction of elastic properties of composites is dependent on the fiber waviness and should be considered. When fibers are slightly misaligned, the influence of fiber waviness becomes insignificant. In the case of 2D-random orientation state, the effect of fiber waviness on the composite's modulus is relatively small. Furthermore, for 3D-random orientation state, the impact of fiber waviness on composite modulus is minimal. Therefore, for fibers with a misaligned orientation state, the effect of fiber waviness on predicting elastic properties of DCFRCs becomes insignificant, especially for a 3D-random orientation.

As already mentioned, the longitudinal stiffness of the unidirectional composite is greatly reduced due to the fiber waviness. Figure 14 illustrates the longitudinal stress distribution in the matrix under the same strain ε_x reinforced by unidirectional straight and curved fibers with the same fiber content. It is evident that the curved fibers increases the stress level of the matrix, indicating the curved fiber reinforced composites may have a lower strength than that of the straight fiber reinforced composites.

3.3 Effect of fiber wavy functions

The influence of fiber wavy functions on the elastic properties of unidirectional composites is also examined. Three distinct types of fiber waviness are considered for the unidirectional composite: half-sine, 3/4-sine, and full sine. For each type of fiber waviness, two different wavy functions are taken into account as

(1) Half-sine:
$$y = f_1(x) = A\sin\left(\frac{\pi}{L}x\right),$$
$$y = f_2(x) = -\frac{4A}{L^2}\left(x - \frac{L}{2}\right)^2 + A,$$

(2) 3/4-sine:
$$y = g_1(x) = -A\sin\left(\frac{3\pi}{2L}x\right),$$
$$y = g_2(x) = -\frac{Ax}{L}\left(\frac{3}{L}x - 2\right)\left(\frac{3}{L}x - 4\right),$$

(3) Full-sine:
$$y = z_1(x) = A\sin\left(\frac{2\pi}{L}x\right),$$
$$y = z_2(x) = \frac{64A}{3L^3}x\left(x - \frac{L}{2}\right)(x - L).$$

The effective composite modulus with different fiber wavy functions for three distinct fiber wavy types is illustrated in Figs. 15-17. It can be observed that, regardless of the fiber wavy type, different wavy functions yield almost identical results. This implies that fiber wavy functions have minimal impact on the properties of composites under a specific fiber wavy type. Additionally, Fig. 15(b) reveals that transverse modulus remains largely unaffected by fiber waviness. This can be attributed to the fact that half-sine wavy type exhibits the least waviness compared to 3/4-sine and full-sine wavy types at the same amplitude A. Furthermore, from Figs. 16(b) and 17(b), it is evident that E_{22} increases with an increase in fiber waviness. Therefore, it can be concluded that the impact of fiber waviness on E_{22} becomes more pronounced as the degree of waviness increases for unidirectional curved fiber composites.

3.4 Modified ROM for DCFRCs

Based on the analysis in Sect. 3.3, it is evident that the

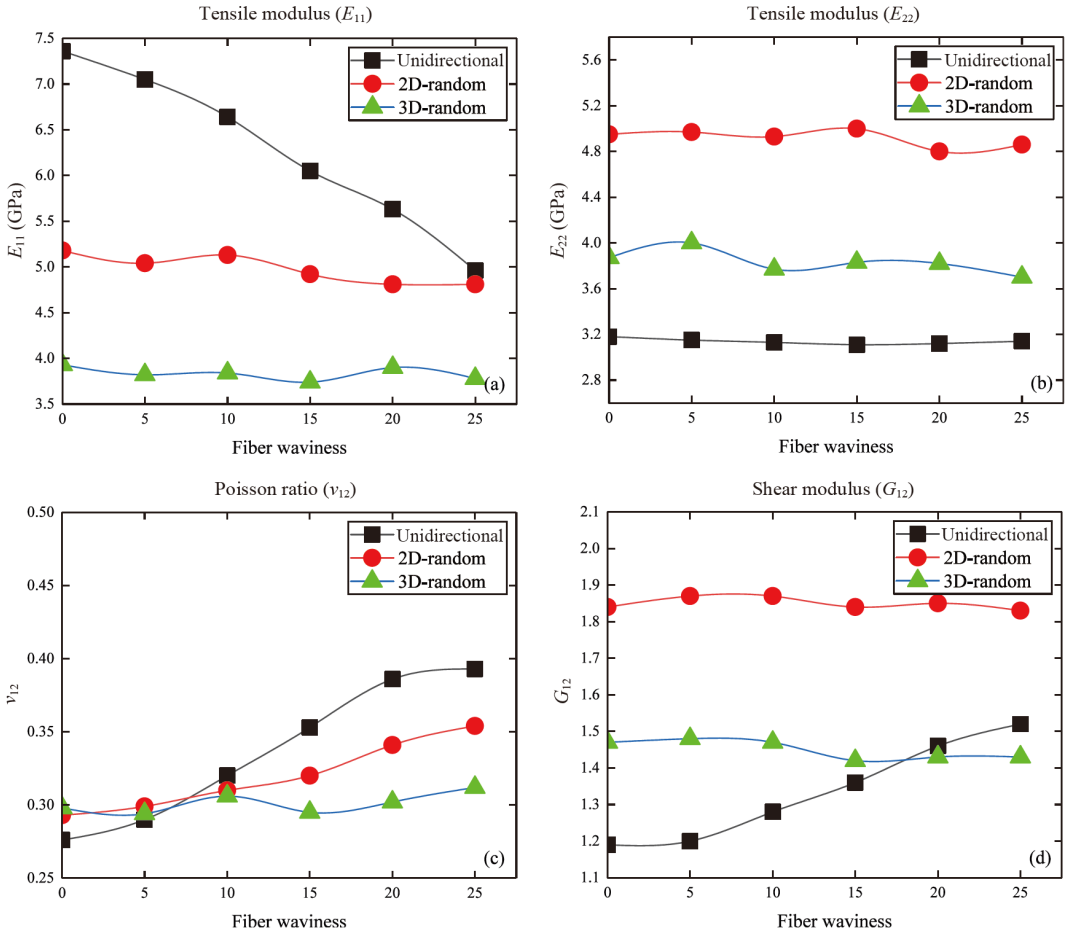

Figure 11 Fiber waviness effects on composite stiffness for half-sine type. (a) E_{11}; (b) E_{22}; (c) ν_{12}; (d) G_{12}.

elastic properties of DCFRCs are primarily influenced by the magnitude of fiber waviness, regardless of the specific mathematical function used to describe the fiber waviness. Therefore, this section aims to adapt the ROM specifically for DCFRCs in order to establish a quantitative relationship between the magnitude of fiber waviness and the elastic properties of DCFRCs.

For the longitudinal modulus of unidirectional DCFRCs, similar to Cox equation, we assume the parameter $\eta_{\mathrm{L}}^{\mathrm{w}}$ as the fiber waviness efficiency factor, representing the influence of fiber waviness on the longitudinal modulus of DCFRCs. This assumption enables us to derive the expression for the longitudinal modulus in curved fiber composites as

$$\begin{cases} E_{\mathrm{L}} = \eta_{\mathrm{L}}\eta_{\mathrm{L}}^{\mathrm{w}} E_{\mathrm{f}} V_{\mathrm{f}} + E_{\mathrm{m}} V_{\mathrm{m}}, \\ \eta_{\mathrm{L}}^{\mathrm{w}} = f(P_{\mathrm{s}}), \end{cases} \tag{18}$$

where P_{s} is the straightness parameter to quantify the tortuosity of a fiber which is introduced by Rezakhaniha et al. [30]. It is defined as the ratio of the end-to-end distance and the actual length of a fiber.

It is important to ensure that the fiber waviness efficiency factor meets the following requirements:

(1) $\eta_{\mathrm{L}}^{\mathrm{w}} = 1$, when $P_{\mathrm{s}} = 1$, which denotes the straight fiber.

(2) $\eta_{\mathrm{L}}^{\mathrm{w}}$ should be an increasing function of P_{s}, which means that smaller P_{s} causes smaller longitudinal modulus.

(3) $\eta_{\mathrm{L}}^{\mathrm{w}}$ is always bigger than zero no matter what value P_{s} takes.

Through the analysis of RVEs, we have successfully derived the expression for the efficiency factor of fiber waviness in relation to longitudinal modulus as

$$\eta_{\mathrm{L}}^{\mathrm{w}} = 1 - \tanh\left(1 - P_{\mathrm{s}} + \sqrt{1 - P_{\mathrm{s}}}\right). \tag{19}$$

The modified ROM for longitudinal modulus of unidirectional DCFRCs is expressed as follows:

$$\begin{cases} E_{\mathrm{L}} = \eta_{\mathrm{L}}\eta_{\mathrm{L}}^{\mathrm{w}} E_{\mathrm{f}} V_{\mathrm{f}} + E_{\mathrm{m}} V_{\mathrm{m}}, \\ \eta_{\mathrm{L}} = 1 - \dfrac{\tanh\left(\dfrac{\beta l}{2}\right)}{\dfrac{\beta l}{2}}, \\ \eta_{\mathrm{L}}^{\mathrm{w}} = 1 - \tanh\left(1 - P_{\mathrm{s}} + \sqrt{1 - P_{\mathrm{s}}}\right). \end{cases} \tag{20}$$

We select the Halpin-Tsai model to calculate the transverse modulus due to its proven high accuracy in predicting

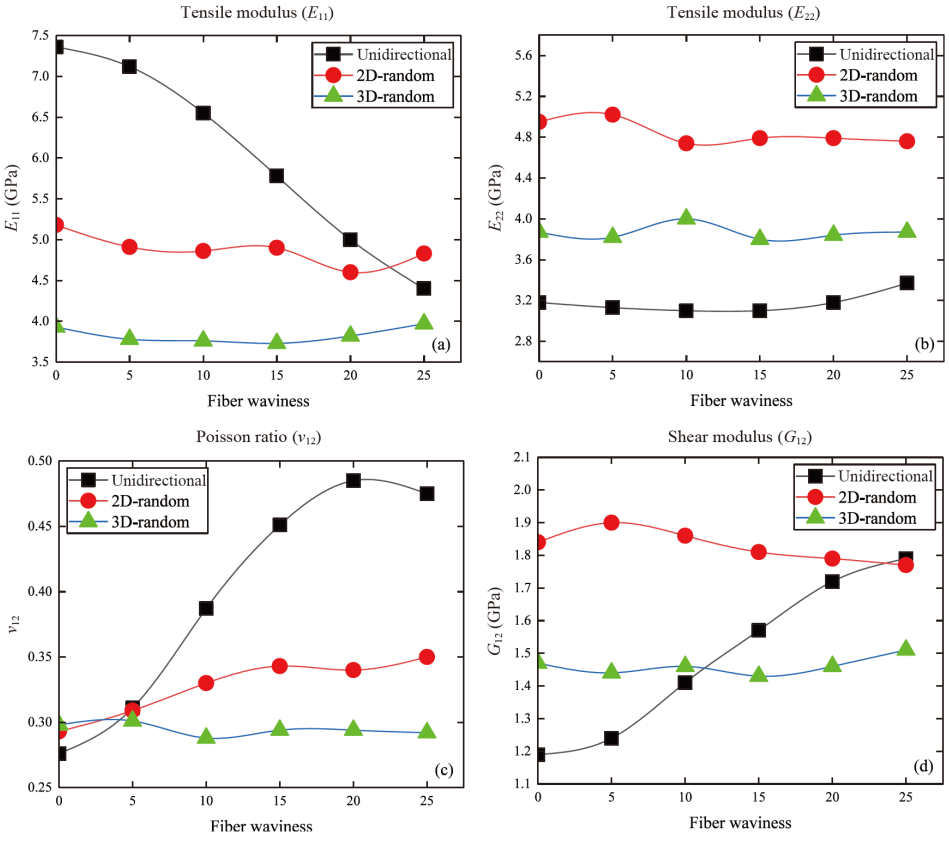

Figure 12 Fiber waviness effects on composite stiffness for 3/4-sine type. (a) E_{11}; (b) E_{22}; (c) v_{12}; (d) G_{12}.

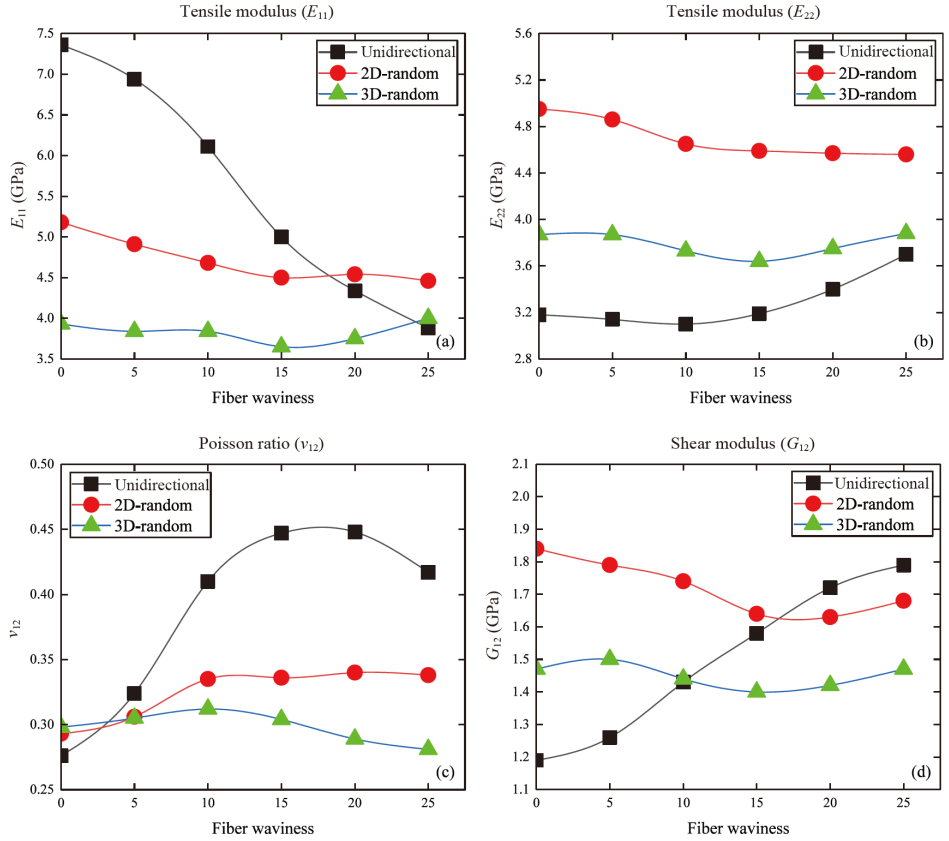

Figure 13 Fiber waviness effects on composite stiffness for full-sine type. (a) E_{11}; (b) E_{22}; (c) v_{12}; (d) G_{12}.

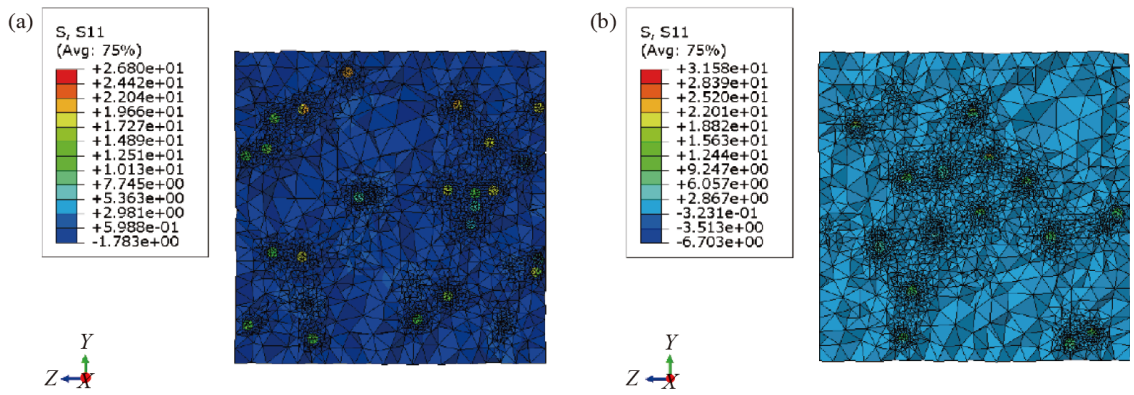

Figure 14 Stress distribution in matrix reinforced by (a) straight fiber and (b) curved fiber under same strain.

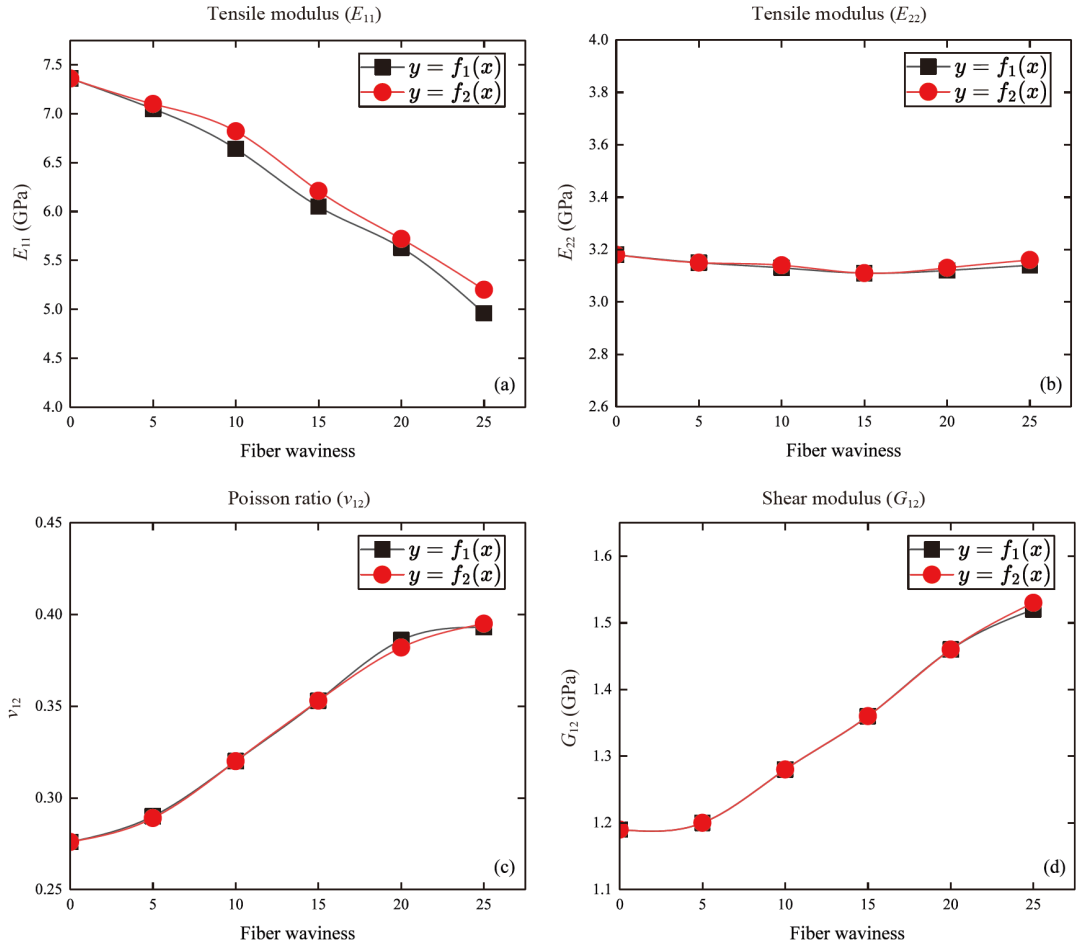

Figure 15 Fiber wavy function effects on composite stiffness for half-sine wavy type. (a) E_{11}; (b) E_{22}; (c) v_{12}; (d) G_{12}.

the behavior of short straight fiber composites. The analysis presented above suggests that the impact of fiber waviness on the transverse modulus of curved fiber composites increases as the level of waviness rises. Similar to the longitudinal modulus, we introduce a factor representing the efficiency of fiber waviness in determining the transverse modulus and derive an expression based on the Rule of Mixture for unidirectional curved fiber composites as follows:

$$\begin{cases} E_{\mathrm{T}} = \dfrac{1+2\eta_{\mathrm{T}}\eta_{\mathrm{T}}^{\mathrm{w}}V_{\mathrm{f}}}{1-\eta_{\mathrm{T}}V_{\mathrm{f}}}E_{\mathrm{m}}, \\ \eta_{\mathrm{T}} = \dfrac{E_{\mathrm{f}}/E_{\mathrm{m}}-1}{E_{\mathrm{f}}/E_{\mathrm{m}}+2}, \\ \eta_{\mathrm{T}}^{\mathrm{w}} = 1+\tanh\left(\dfrac{1-P_{\mathrm{s}}+\sqrt{1-P_{\mathrm{s}}}}{2}\right), \end{cases} \tag{21}$$

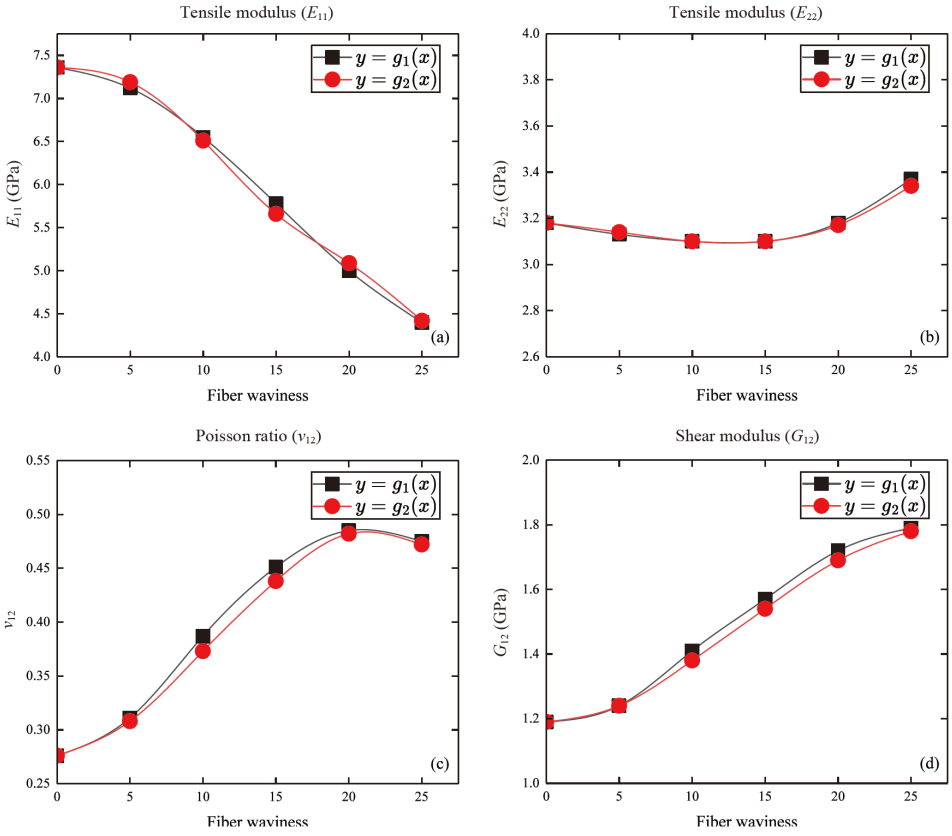

Figure 16 Fiber wavy function effects on composite stiffness for 3/4-sine wavy type. (a) E_{11}; (b) E_{22}; (c) v_{12}; (d) G_{12}.

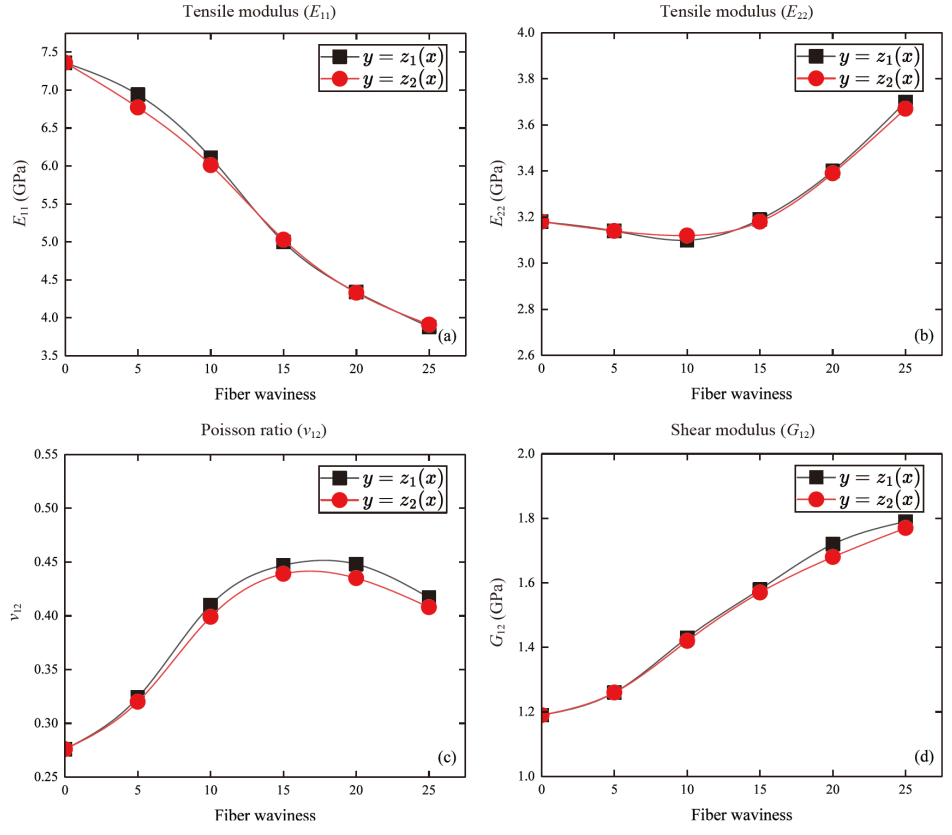

Figure 17 Fiber wavy function effects on composite stiffness for full-sine wavy type. (a) E_{11}; (b) E_{22}; (c) v_{12}; (d) G_{12}.

where $\eta_{\mathrm{T}}^{\mathrm{w}}$ is the fiber waviness efficiency factor for transverse modulus.

For a 2D-random distribution state, the effect of fiber waviness on the elastic properties of composites is found to be smaller than that of the composite with a unidirectional fiber distribution. Through analysis of the results obtained from the RVE, we can obtain

2D-random

$$\begin{cases} E_{\mathrm{c}} = \dfrac{3}{8}\eta_{2\mathrm{D}}^{\mathrm{w}} E_{\mathrm{L}} + \dfrac{5}{8}E_{\mathrm{T}}, \\ \eta_{2\mathrm{D}}^{\mathrm{w}} = 1 + \tanh\left(\dfrac{1-P_{\mathrm{s}}+\sqrt{1-P_{\mathrm{s}}}}{2}\right), \end{cases} \tag{22}$$

where $\eta_{2\mathrm{D}}^{\mathrm{w}}$ is the fiber waviness efficiency factor for 2D-random orientation state.

The elastic properties of composites in a 3D-random distribution state are minimally affected by fiber waviness, making them similar to composites with short straight fibers

3D-random

$$E_{\mathrm{c}} = \frac{1}{5}E_{\mathrm{L}} + \frac{4}{5}E_{\mathrm{T}}, \tag{23}$$

where E_{L} and E_{T} denote the longitudinal and transverse modulus for unidirectional curved fiber composites with the same fiber waviness, fiber diameter, fiber aspect ratio and fiber content, obtained from Eqs. (20) and (21) respectively.

The modulus values obtained using ROM are compared with the results from RVEs to validate the accuracy of the ROM, considering different fiber orientations, fiber content fractions, and fiber waviness. The comparative findings are presented in Figs. 18-20. Only one wavy function for each wavy type is selected as

(1) Half-sine: $y = f_1(x) = A\sin\left(\dfrac{\pi}{L}x\right)$,

(2) 3/4-sine: $y = g_1(x) = -A\sin\left(\dfrac{3\pi}{2L}x\right)$,

(3) Full-sine: $y = z_1(x) = A\sin\left(\dfrac{2\pi}{L}x\right)$.

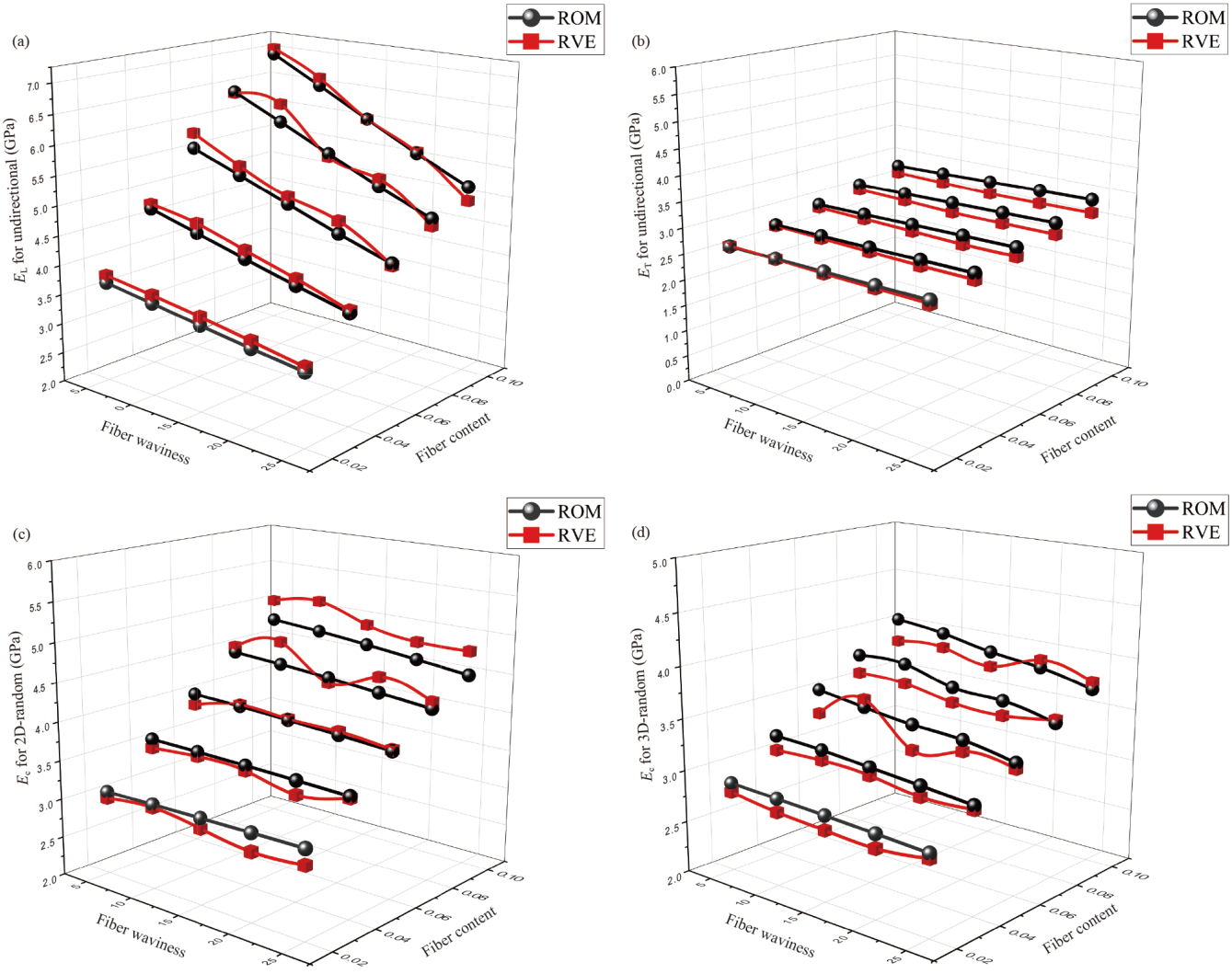

Figure 18 Results comparison of ROM with RVE for half-sine wavy type. (a) Longitudinal modulus for unidirectional state; (b) transverse modulus for unidirectional state; (c) elastic modulus for 2D-random state; (d) elastic modulus for 3D-random state.

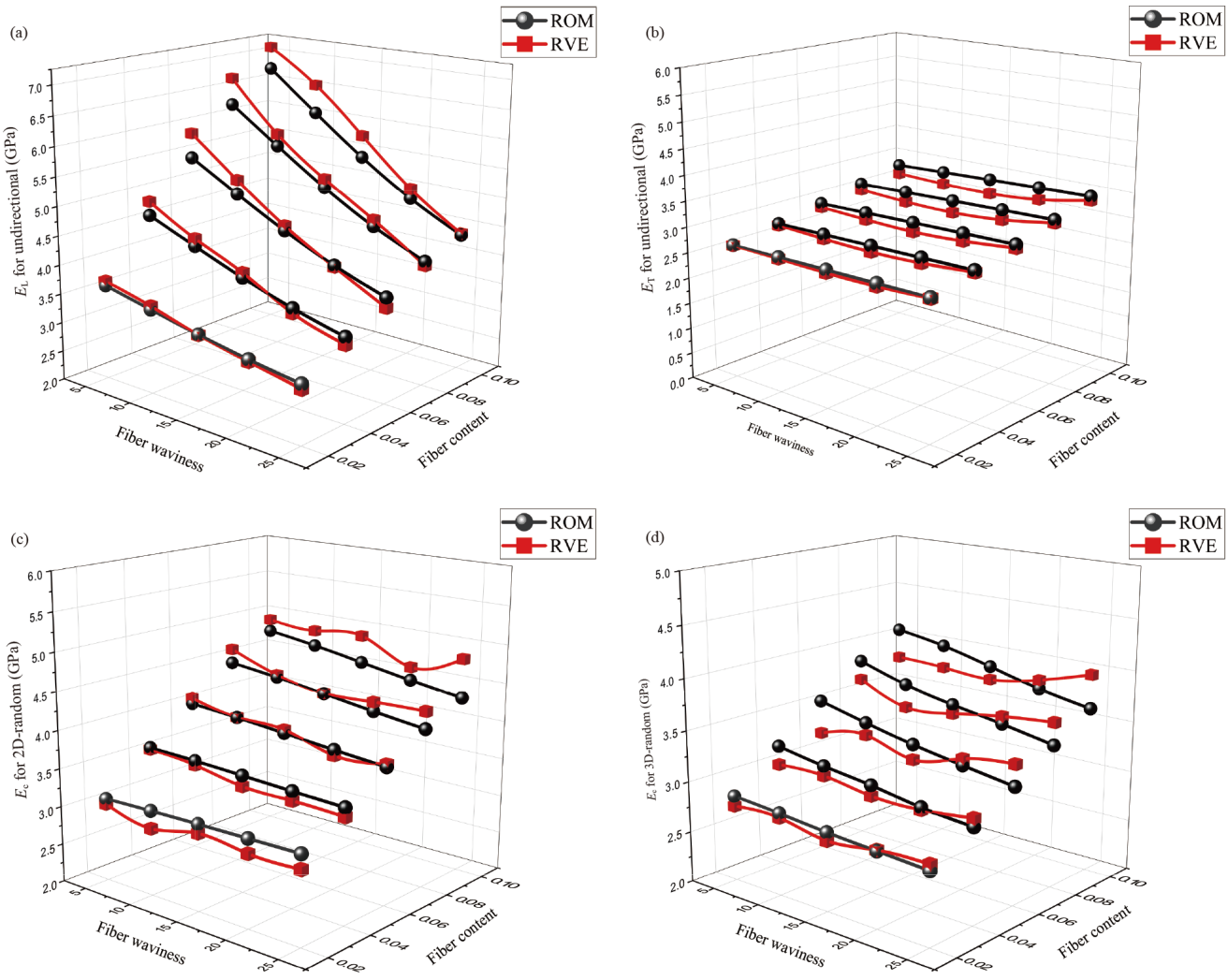

Figure 19 Results comparison of ROM with RVE for 3/4-sine wavy type. (a) Longitudinal modulus for unidirectional state; (b) transverse modulus for unidirectional state; (c) elastic modulus for 2D-random state; (d) elastic modulus for 3D-random state.

The straightness parameters P_s for every wavy function are shown as Table 5.

The comparison results demonstrate the excellent predictive accuracy of the proposed ROM for the primary elastic modulus of discontinuous curved fiber composites across various orientation states. In the unidirectional state, the maximum error is approximately 10%. For 2D-random fiber alignment, although there is a maximum prediction error of 11.3%, most errors fall within an acceptable range below 10%. The ROM exhibits remarkable predictive accuracy for 3D-random fiber alignment, with majority errors remaining within a tolerable limit of 10%.

4. Conclusion

A modified RSA algorithm to generate RVEs for DCFRCs has been presented, and the influences of fiber waviness and waviness function on the elastic properties of the composite have been examined. Subsequently, a modified ROM has been proposed. The following conclusions can be drawn:

(1) The proposed modified RSA algorithm can easily generate the RVE of DCFRCs with various waviness functions. The maximum achievable fiber volume fraction can reach 15% with a fiber aspect ratio of 15. The comparison between RVE results and experimental results has demonstrated its validation.

(2) The influence of fiber waviness on E_{22} is significant only when the magnitude of fiber waviness is large, as revealed by the effect analysis of fiber waviness on composite properties.

(3) The proposed modified ROM can be utilized for predicting the elastic modulus of DCFRCs with varying fiber orientation and content. The predicted results of ROM demonstrate good agreement with the RVE results, providing an efficient method for predicting the elastic modulus of DCFRCs.

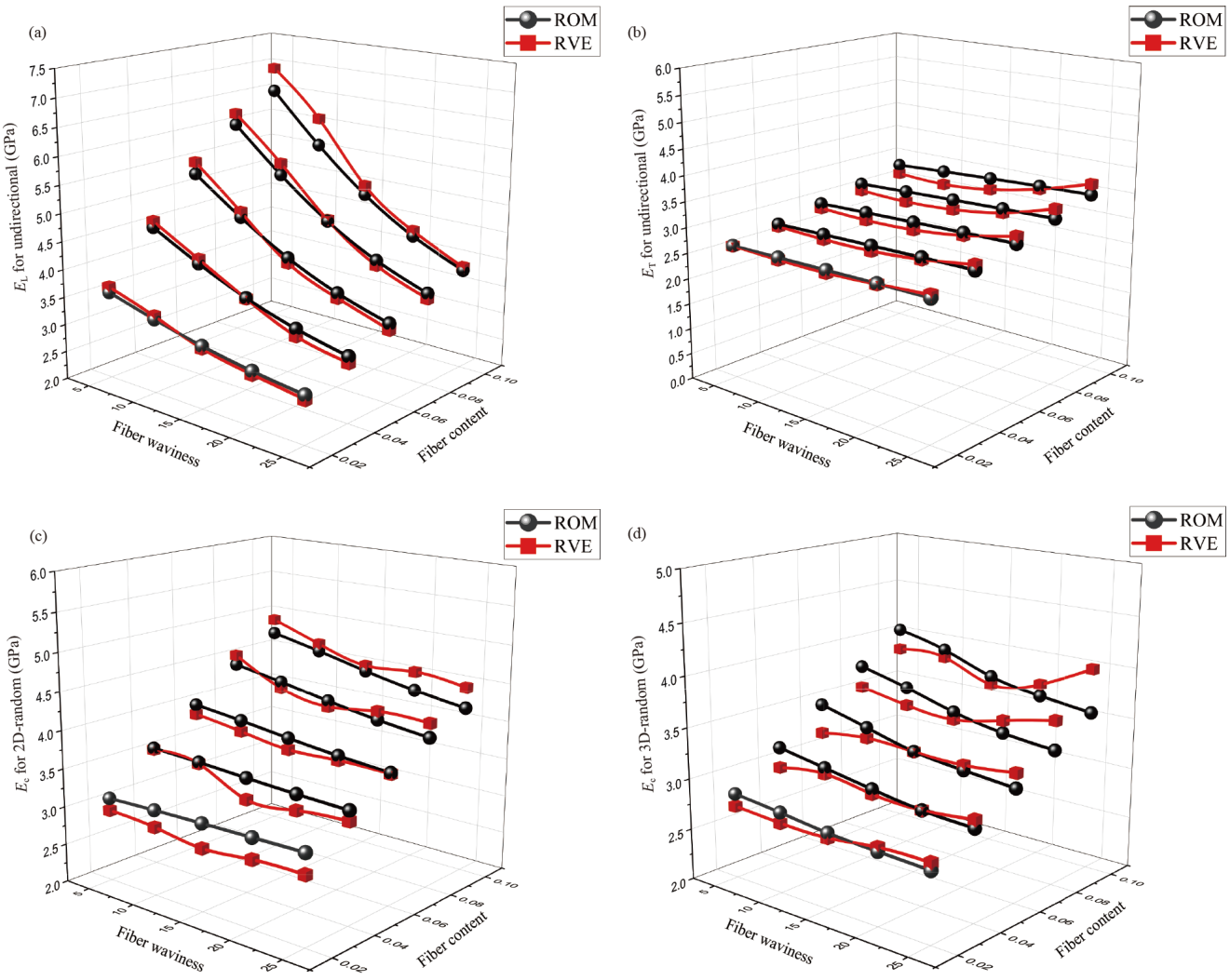

Figure 20 Results comparison of ROM with RVE for full-sine wavy type. (a) Longitudinal modulus for unidirectional state; (b) transverse modulus for unidirectional state; (c) elastic modulus for 2D-random state; (d) elastic modulus for 3D-random state.

Table 5 Straightness parameters for every wavy function

Wavy function	Wavy amplitude A	Straightness parameter
$y=f_1(x)$ $=A\sin\left(\frac{\pi}{L}x\right)$	5	0.9945
	10	0.9785
	15	0.9537
	20	0.9223
	25	0.8866
$y=g_1(x)$ $=-A\sin\left(\frac{3\pi}{2L}x\right)$	5	0.9877
	10	0.9537
	15	0.9049
	20	0.8488
	25	0.7911
$y=z_1(x)$ $=A\sin\left(\frac{2\pi}{L}x\right)$	5	0.9785
	10	0.9223
	15	0.8488
	20	0.7721
	25	0.7001

Conflict of interest *On behalf of all authors, the corresponding author states that there is no conflict of interest.*

Author contributions ***Wujie Chen****: Writing – original draft, Visualization, Methodology, Investigation, Software, Formal analysis.* ***Kunkun Fu****: Writing – review & editing, Supervision, Project administration, Resources, Funding acquisition, Conceptualization.* ***Yan Li****: Writing – review & editing, Supervision, Project administration, Resources, Funding acquisition, Conceptualization.*

Acknowledgements *This work was supported by the Liaoning Science and Technology Program "Open Bidding for Selecting the Best Candidates" Project, China (Grant No. 2022JH1/10400043), and Shanghai Science and Technology Innovation Action Plan, China (Grant No. 22511102600). This research was also sponsored by Shanghai Gaofeng Project for University Academic Program Development.*

1 B. Du, Z. Li, H. Bai, Q. Li, C. Zheng, J. Liu, F. Qiu, Z. Fan, H. Hu, and L. Chen, Mechanical property of long glass fiber reinforced polypropylene composite: From material to car seat frame and bumper beam, Polymers **14**, 1814 (2022).

2 M. Wang, J. Du, M. Li, F. Pierini, X. Li, J. Yu, and B. Ding, *In situ* forming double-crosslinked hydrogels with highly dispersed short fibers for the treatment of irregular wounds, Biomater. Sci. **11**, 2383 (2023).

3 H. Ning, S. Pillay, K. B. Thattaiparthasarathy, and U. K. Vaidya, Design and manufacturing of long fiber thermoplastic composite

helmet insert, Compos. Struct. **168**, 792 (2017).
4 F. Felline, P. Conte, R. Rametta, A. Migali, O. Manni, L. Barone, and A. Maffezzoli, Long fiber pp-glass composites for the design and manufacturing of a recyclable sail boat, WIT Trans. Built Environ. **68**, 49-58 (2003).
5 P. J. Hine, H. Rudolf Lusti, and A. A. Gusev, Numerical simulation of the effects of volume fraction, aspect ratio and fibre length distribution on the elastic and thermoelastic properties of short fibre composites, Compos. Sci. Technol. **62**, 1445 (2002).
6 B. Jiang, C. Liu, C. Zhang, B. Wang, and Z. Wang, The effect of non-symmetric distribution of fiber orientation and aspect ratio on elastic properties of composites, Compos. Part B-Eng. **38**, 24 (2007).
7 D. A. Jack, and D. E. Smith, Elastic properties of short-fiber polymer composites, derivation and demonstration of analytical forms for expectation and variance from orientation tensors, J. Compos. Mater. **42**, 277 (2008).
8 P. Pinter, B. Bertram, and K. A. Weidenmann, in A novel method for the determination of fibre length distributions from µCT-data: Proceedings of 6th Conference on Industrial Computed Tomography (ICT), Wels, Austria, 2016.
9 D. Qian, E. C. Dickey, R. Andrews, and T. Rantell, Load transfer and deformation mechanisms in carbon nanotube-polystyrene composites, Appl. Phys. Lett. **76**, 2868 (2000).
10 S. Bapanapalli, and B. N. Nguyen, Prediction of elastic properties for curved fiber polymer composites, Polym. Compos. **29**, 544 (2008).
11 C. Tsai, C. Zhang, D. A. Jack, R. Liang, and B. Wang, The effect of inclusion waviness and waviness distribution on elastic properties of fiber-reinforced composites, Compos. Part B-Eng. **42**, 62 (2011).
12 S. Oller, L. G. Nallim, F. J. Bellomo, and G. Ruano, A theoretical homogenized constitutive model formulation for matrix composite materials reinforced with curved fibers, Compos. Struct. **304**, 116432 (2023).
13 H. Altendorf, and D. Jeulin, Random-walk-based stochastic modeling of three-dimensional fiber systems, Phys. Rev. E **83**, 041804 (2011).
14 S. Herasati, and L. Zhang, A new method for characterizing and modeling the waviness and alignment of carbon nanotubes in composites, Compos. Sci. Tech. **100**, 136 (2014).
15 A. Kumar, A. DasGupta, and A. Jain, Microstructure generation algorithm and micromechanics of curved fiber composites with random waviness, Int. J. Solids Struct. **289**, 112625 (2024).
16 M. Schneider, An algorithm for generating microstructures of fiber-reinforced composites with long fibers, Int. J. Numer. Methods Eng. **123**, 6197 (2022).
17 R. Velmurugan, G. Srinivasulu, and S. Jayasankar, Influence of fiber waviness on the effective properties of discontinuous fiber reinforced composites, Comp. Mater. Sci. **91**, 339 (2014).
18 J. F. Zhang, X. X. Zhang, Z. Y. Liu, Q. Z. Wang, B. L. Xiao, and Z. Y. Ma, A rigid body dynamics simulation enhanced representative volume element builder for CNT/Al composite, Int. J. Mech. Mater. Des. **18**, 407 (2022).
19 Y. Abdin, S. V. Lomov, A. Jain, G. H. van Lenthe, and I. Verpoest, Geometrical characterization and micro-structural modeling of short steel fiber composites, Compos. Part A-Appl. Sci. Manuf. **67**, 171 (2014).
20 H. L. Cox, The elasticity and strength of paper and other fibrous materials, Br. J. Appl. Phys. **3**, 72 (1952).
21 J. C. Halpin, Effects of Environmental Factors on Composite Materials, Technical Report (Defense Technical Information Center, 1969).
22 C. C. Chamis, F. Abdi, M. Garg, L. Minnetyan, H. Baid, D. Huang, J. Housner, and F. Talagani, Micromechanics-based progressive failure analysis prediction for WWFE-III composite coupon test cases, J. Compos. Mater. **47**, 2695 (2013).
23 B. Tonpheng, J. Yu, B. M. Andersson, and O. Andersson, Tensile strength and young's modulus of polyisoprene/single-wall carbon nanotube composites increased by high pressure cross-linking, Macromolecules **43**, 7680 (2010).
24 Y. Zare, and H. Garmabi, Attempts to simulate the modulus of polymer/carbon nanotube nanocomposites and future trends, Polym. Rev. **54**, 377 (2014).
25 W. Tian, L. Qi, J. Zhou, J. Liang, and Y. Ma, Representative volume element for composites reinforced by spatially randomly distributed discontinuous fibers and its applications, Compos. Struct. **131**, 366 (2015).
26 A. Chanda, S. K. Sinha, and N. V. Datla, The influence of fiber alignment, structure and concentration on mechanical behavior of carbon nanofiber/epoxy composites: Experimental and numerical study, Polym. Compos. **42**, 1155 (2021).
27 S. M. Mirkhalaf, E. H. Eggels, T. J. H. van Beurden, F. Larsson, and M. Fagerström, A finite element based orientation averaging method for predicting elastic properties of short fiber reinforced composites, Compos. Part B-Eng. **202**, 108388 (2020).
28 J. Nafar Dastgerdi, M. Lotf Yasouri, and H. Hosseini Toudeshky, Microstructure-sensitive investigation on the mechanical behavior of CNT-reinforced composites considering debonding damage based on cohesive finite element method, Mater. Today Commun. **31**, 103458 (2022).
29 K. Xiao, L. Zhang, and I. Zarudi, Mechanical and rheological properties of carbon nanotube-reinforced polyethylene composites, Compos. Sci. Tech. **67**, 177 (2007).
30 R. Rezakhaniha, A. Agianniotis, J. T. C. Schrauwen, A. Griffa, D. Sage, C. V. C. Bouten, F. N. van de Vosse, M. Unser, and N. Stergiopulos, Experimental investigation of collagen waviness and orientation in the arterial adventitia using confocal laser scanning microscopy, Biomech. Model. Mechanobiol. **11**, 461 (2012).

一种建立不连续弯曲纤维复合材料RVE的改进的随机序列吸附算法

陈吴杰, 付昆昆, 李岩

摘要 为了预测具有不同纤维弯曲函数和纤维取向的不连续弯曲纤维复合材料(DCFRCs)的弹性性能, 本文提出了一种改进的随机序列吸附(RSA)算法, 以生成不连续弯曲纤维复合材料的代表体积单元(RVE)模型. 通过引入一种小移动方法来改进传统的RSA算法. 与传统的RSA算法相比, 改进后的RSA算法的生成效率提高了40%以上. 当纤维长径比为15时, 可实现的最大纤维体积分数为15%. 利用所建立的RVE模型进行有限元分析, 研究了纤维弯曲大小和弯曲函数对DCFRCs弹性性能的影响. 最后, 提出了一种改进的混合规则来预测不同纤维取向的DCFRCs的弹性性能. 结果表明, 修正的混合规则预测的弹性性能与RVE模型的预测结果吻合较好, 证明了修正的混合规则的有效性.